Journal of the Korean Crystal Growth and Crystal Technology
Vol. 14, No. 4 (2004) 160-168

Lead bromide crystal growth from the melt and characterization: the effects of nonlinear thermal boundary conditions on convection during physical vapor crystal growth of mercurous bromide

Geug-Tae Kim† and Moo Hyun Kwon*

Department of Nano-Bio Chemical Engineering, Hannam University, Taejon 306-791, Korea
**Department of Chemical Engineering, Woosuk University, Jeonbuk 565-701, Korea*

(Received July 19, 2004)
(Accepted July 29, 2004)

Abstract We investigate the effects of solutal convection on the crystal growth rate in a horizontal configuration for diffusive-convection conditions and purely diffusion conditions achievable in a low gravity environment for a nonlinear thermal gradient. It is concluded that the solutally-driven convection due to the disparity in the molecular weights of the component A (Hg_2Br_2) and B (CO) is stronger than thermally-driven convection for both the nonlinear and the linear thermal profiles, corresponding to $Gr_t = 8.5\times10^3$, $Gr_s = 1.05\times10^5$. For both solutal and thermal convection processes, the growth rates for the linear thermal profile (conducting walls) are greater than for the nonlinear case. With the temperature humps, there are found to be observed in undersaturation for diffusive-convection processes ranging from $D_{AB} = 0.087$ to 0.87. For the vertical configurations, the diffusion mode is so much dominated that the growth rate and interfacial distribution is nearly regardless of the gravitational accelerations. Also, the diffusion mode is predominant over the convection for the gravity levels less than 0.1 g_0 for the horizontally oriented configuration.

Key words Mercurous bromide, Solutal convection, Physical vapor transport

1. Introduction

Interest in growing Hg_2Br_2 single crystal stems from their exceptional optical properties and very broad transmission range from 0.30 to 30 for applications in acousto-optic and opto-electronic devices such as Bragg cells, X-ray detectors operating at ambient temperature [1]. The solid-liquid equilibrium data on the mercuric bromide ($HgBr_2$) and mercury (Hg) system has not been studied extensively. The available phase diagram [2] suggests that equimolar compound Hg_2Br_2 decomposes to two liquids at a temperature near 450°C where the vapor pressure is well above 20 atm. Because of this decomposition and high vapor pressure, mercurous bromide cannot be solidified as a single crystal directly from the stoichiometric melt. However, very similar to the mercurous chloride, mercurous bromide exhibits sufficiently high vapor pressure at low temperatures so that these crystals are usually grown by the physical vapor transport (PVT) in closed silica glass ampoules. The PVT processing has many advantages over melt-growth methods since it can be conducted at low temperatures: (1) vapor-solid interfaces possess relatively high interfacial morphological stability against non-uniformities in heat and mass transfer; (2) high purity crystals are achieved; (3) materials decomposed before melting, such as Hg_2Br_2 can be grown; (4) lower point defect and dislocation densities are achieved [3]. The mechanism of the PVT process is simple: sublimation-condensation in closed silica glass ampoules in temperature gradient imposed between the source material and the growing crystal. In the PVT system of Hg_2Br_2, the molecular species Hg_2Br_2 sublimes as the vapor phase from the crystalline source material (Hg_2Br_2), and is subsequently transported and re-incorporated into the single crystalline phase (Hg_2Br_2) [4]. Recently PVT has become an important crystal growth process for a variety of acousto-optic materials. However, the industrial applications of the PVT process remain limited. An important main reason is that transport phenomena occurring in the vapor are complex and coupled so that it is difficult to design or control the process accurately. Such complexity and coupling are associated with the inevitable occurrence of thermal convection generated by the interaction of gravity with density gradients arising from temperature gradients. Thermal convection has been regarded as detrimental and, thus, to be avoided or minimized in PVT growth system. These thermal convec-

†Corresponding author
Tel: +82-42-629-7984
Fax: +82-42-623-9489
E-mail: gtkim@hannam.ac.kr

tion-induced complications result in problems ranging from crystal inhomogeneity to structural imperfection. Therefore, in order to analyze and control the PVT process accurately, and also make significant improvements in the process, it is essential to investigate the roles of thermal convection in the PVT process.

Markham, Greenwell and Rosenberger [5] examined the effects of thermal and thermosolutal convections during the PVT process inside vertical cylindrical enclosures for a time-independent system, and showed that even in the absence of gravity, convection can be present, causing nonuniform concentration gradients. They emphasized the role of geometry in the analysis of the effects of convection. As such these fundamentally constitute steady state two-dimensional models. The steady state models are limited to low Rayleigh number applications, because as the Rayleigh number increases oscillation of the flow field occurs. To address the issue of unsteady flows in PVT, Duval [6] performed a numerical study on transient thermal convection in the PVT processing of Hg_2Cl_2 very similar to the mercurous bromide for a vertical rectangular enclosure with insulated temperature boundary conditions for Rayleigh numbers up to 10^6. Duval [7] has also shown the bifurcation sequences which lead to chaotic flow in PVT processing. Nadarajah *et al.* [8] addressed the effects of solutal convection for any significant disparity in the molecular weights of the crystal components and the inert gas. Zhou *et al.* [9] reported that the traditional approach of calculating the mass flux assuming one-dimensional flow for low vapor pressure systems is indeed correct. Rosenberger *et al.* [10] studied three-dimensional numerical modeling of the PVT yielded quantitative agreement with measured transport rates of iodine through octofluorocyclobutane (C_4F_8) as inert background gas in horizontal cylindrical ampoules.

In this numerical study, a two-dimensional model is used for the analysis of the PVT processes during vapor-growth of mercurous bromide crystals (Hg_2Br_2) in horizontally oriented, cylindrical, closed ampoules in a two-zone furnace system. Mass transfer-limited processes are considered in this paper, although the recent paper of Singh, Mazelsky and Glicksman [11] demonstrated that the interface kinetics plays an important role in the PVT system of Hg_2Cl_2 very similar to the mercurous bromide. Solutal convection will be considered at this point, primarily because a mixture of Hg_2Br_2 vapor contain some impurity such as carbon monoxide and thermal convection can be ignored in comparison to solutally-induced convection for imposed nonlinear thermal profile to prevent supersaturation along the transport path.

It is the purpose of this paper (1) to discuss the development of a mathematical model for single crystals inside a PVT reactor, incorporating the mass transfer-limited model with idealized boundary conditions, (2) to relate the applied convective process parameters to crystal growth rate and its interfacial distributions, (3) to examine the effects of solutal convection with a nonlinear and a linear temperature profile in order to gain insights into the underlying physicochemical processes.

2. The Model

Consider a rectangular enclosure of height H and transport length L, shown in Fig. 1. The source is maintained at a temperature T_s, while the growing crystal is at a temperature T_c, with $T_s > T_c$. PVT of the transported component A (Hg_2Br_2) occurs inevitably, due to presence of impurities, with the presence of an inert component B (CO). The interfaces are assumed to be flat for simplicity. The finite normal velocities at the interfaces can be expressed by Stefan flow deduced from the one-dimensional diffusion-limited model [12], which provide the coupling between the fluid dynamics and species calculations. On the other hand, the tangential component of the mass average velocity of the vapor at the interfaces vanishes. Thermodynamic equilibria are assumed at the interfaces so that the mass fractions at the interfaces are kept constant at $\omega_{A,s}$ and $\omega_{A,c}$. On the vertical non-reacting walls an appropriate velocity boundary condition is no-slip, the normal concentration gradient is zero, and temperature is imposed as a linear temperature gradient and an asymmetric horizontal temperature gradient. The asymmetry is attributable to temperature differences between two opposite walls.

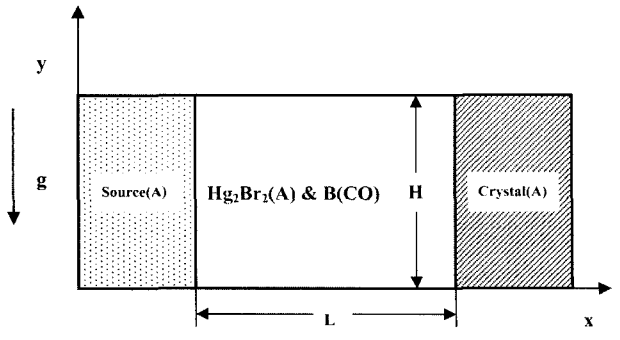

Fig. 1. Schematic of PVT growth reactor in a two-dimensional rectangular system.

Thermophysical properties of the fluid are assumed to be constant, except for the density. When the Boussinesq approximation is invoked, density is assumed constant except the buoyancy body force term. The density is assumed to be a function of temperature and not of concentration. The ideal gas law and Dalton's law of partial pressures are used. Viscous energy dissipation and the Soret-Dufour (thermo-diffusion) effects can be neglected, as their contributions remain relatively insignificant for the conditions encountered in our PVT crystal growth processes. Radiative heat transfer can be neglected under our conditions, based on Kassemi and Duval [13].

The transport of fluid within a rectangular PVT crystal growth reactor is governed by a system of elliptic, coupled conservation equations for mass (continuity), momentum, energy and species (diffusion) with their appropriate boundary conditions. Let v_x, v_y denote the velocity components along the x- and y-coordinates in the x, y rectangular coordinate, and let T, ω_A, p denote the temperature, mass fraction of species A (Hg_2Br_2) and pressure, respectively.

The dimensionless variables are scaled as follows:

$$x^* = \frac{x}{H},\quad y^* = \frac{y}{H}, \tag{1}$$

$$u = \frac{u_x}{U_c},\quad v = \frac{v_y}{U_c},\quad p = \frac{p}{\rho_c U_c^2}, \tag{2}$$

$$T^* = \frac{T-T_c}{T_s-T_c},\quad \omega_A^* = \frac{\omega_A-\omega_{A,c}}{\omega_{A,s}-\omega_{A,c}}. \tag{3}$$

$$\nabla^*\bullet\nabla^* = 0, \tag{4}$$

$$\vec{V}^*\bullet\nabla^*\vec{V}^* = -\nabla^* p^* + Pr\nabla^{*2}\vec{V}^* - Ra\cdot Pr\cdot T^*\cdot e_g, \tag{5}$$

$$\vec{V}^*\bullet\nabla^* T^* = \nabla^{*2} T^* \tag{6}$$

$$\vec{V}^*\bullet\nabla^*\omega_A^* = \frac{1}{Le}\nabla^{*2}\omega_A^* \tag{7}$$

The dimensionless governing equations are given by:

These nonlinear, coupled sets of equations are numerically integrated with the following boundary conditions:

On the walls ($0 < x^* < L/H$, $y^* = 0$ and 1):

$$u(x^*,0) = u(x^*,1) = v(x^*,0) = v(x^*,1) = 0 \tag{8}$$

$$\frac{\partial\omega_A^*(x^*,0)}{\partial y^*} = \frac{\partial\omega_A^*(x^*,1)}{\partial y^*} = 0,$$

$$T^*(x^*,0) = T^*(x^*,1) = \frac{T-T_c}{T_s-T_c}$$

On the source ($x^* = 0$, $0 < y^* < 1$):

$$u(0,y^*) = -\frac{1}{Le(1-\omega_{A,s})}\frac{\Delta\omega}{}\frac{\partial\omega_A^*(0,y^*)}{\partial x^*}, \tag{9}$$

$$v(0,y^*) = 0,$$

$$T^*(0,y^*) = 1,$$

$$\omega_A^*(0,y^*) = 1.$$

On the crystal ($x^* = L/H$, $0 < y^* < 1$):

$$u(L/H,y^*) = -\frac{1}{Le(1-\omega_{A,c})}\frac{\Delta\omega}{}\frac{\partial\omega_A^*(L/H,y^*)}{\partial x^*}, \tag{10}$$

$$v(L/H,y^*) = 0,$$

$$T^*(L/H,y^*) = 0,$$

$$\omega_A^*(L/H,y^*) = 0.$$

The following temperature profile was used as a boundary condition along the ampoule (y = 0 and y = H): this equation is expressed in reference to an approximate fit of experimental data [14, 15], see Fig. 2.

$$T(t) = \begin{cases} 563.16 & \text{for } -20\le t\le -10 \text{ cm} \\ 608 + 4.97t - 0.70t^2 & \text{for } -10\le t\le 12 \text{ cm} \\ -5.91\times10^{-2}t^3 & \\ +\ 6.67\times10^{-3}t^4 & \\ +\ 2.60\times10^{-4}t^5 & \\ -2.49\times10^{-5}t^6 & \\ 593.16 & \text{for } 12\le t\le 20 \text{ cm} \end{cases} \tag{11}$$

Relative to Fig. 2, during the crystal growth the ampoule is placed in the nonlinear thermal profile as shown in Fig. 3. The hump region corresponds to the location of the vapor component A and B inside the

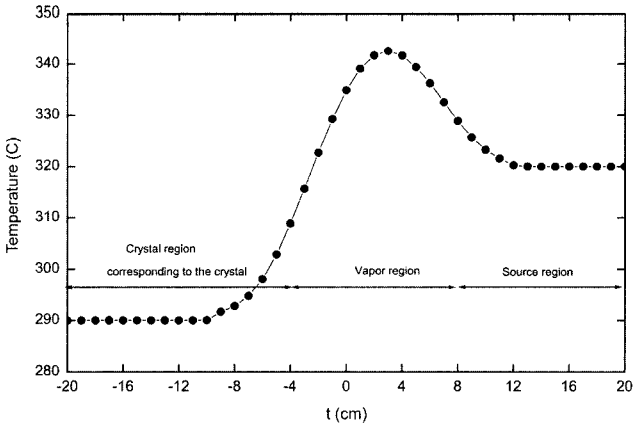

Fig. 2. Temperature profile along the ampoule.

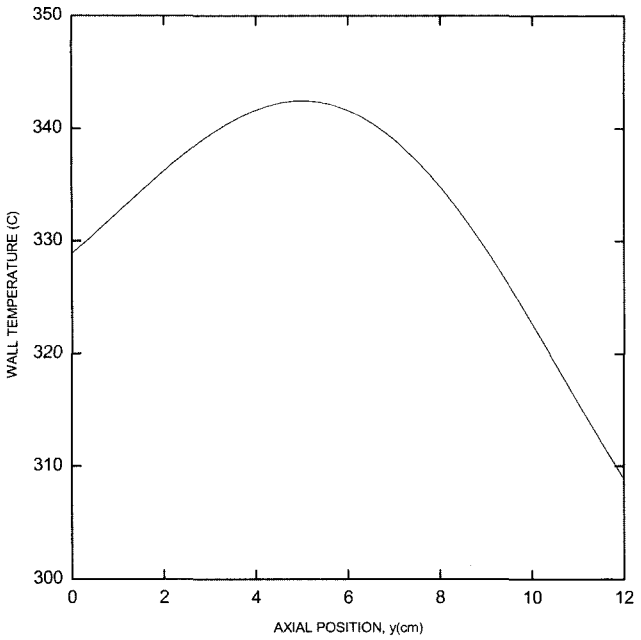

Fig. 3. Axial temperature profile given by Eq. (11) with maximum ("hump") between T_s and T_c.

ampoule. The source material lies in the region with the larger temperature near t ≥ 8 cm. Whereas crystal growth occurs in the region corresponding to t ≤ –4 cm. In our experiments we position the ampoule in the growth region with a temperature less than the source in order to drive the process. In addition, the length of the hump region can also be adjusted so that we have a much larger source region. With respect to Fig. 3, the following transformation is used to relate the laboratory reference to the ampoule: where K_i is

$$x = K_i - t$$

the position of the source and vapor interface in the laboratory reference frame.

In the dimensionless parameters in the governing equations the thermophysical properties of the gas mixture are estimated from gas kinetic theory using Chapman-Enskog's formulas [16].

The vapor pressure [17] p_A of Hg_2Br_2 (in the unit of Pascal) can be evaluated from the

$$p_A = e^{(a - b/T)},$$

following formula as a function of temperature: in which a = 29.75, b = 11767.1.

The crystal growth rate V_c is calculated from a mass balance at the crystal vapor interface, assuming fast kinetics, i.e. all the vapor is incorporated into the crystal, which is given by (subscripts c, v refer to crystal and vapor respectively)

$$\int \rho_v u_v \cdot ndA = \int \rho_c u_c \cdot ndA, \tag{13}$$

$$u_c = \frac{\rho_v \int u_v \cdot ndA}{\rho_v \int dA}. \tag{14}$$

The detailed numerical schemes in order to solve the discretization equations for the system of nonlinear, coupled governing partial differential equations are found in [18].

3. Results and Discussion

The parametric study is useful for showing trends and generalizing the problem, but many parameters are involved in the problem under consideration, which renders it difficult for a general analysis. One of the purposes for this study is to correlate the growth rate and the interfacial distributions to process parameters for a particular material (Hg_2Br_2). Thus, it is desirable to express some results in terms of dimensional growth rate, however they are also applicable to parameter ranges over which the process varies in the manner given. The six dimensionless parameters, namely Gr, Ar, Pr, Le, C_v and Pe, are independent and arise naturally from the dimensionless governing equations and boundary conditions. The dimensionless parameters and physical properties for the operating conditions of this study are shown in Table 1.

In this study, the effects of the solutal convection and gravitational acceleration perturbations on the crystal growth and its distributions across an interface. Residual gas such as carbon monoxide in PVT processes

Table 1
Typical thermo-physical properties used in simulations (M_A = 560.988, M_B = 28)

Transport length, L	12 cm
Height, H	2 cm
Source temperature, T_s	329°C
Crystal temperature, T_c	309°C
Density, ρ	0.0016 g/cm^3
Dynamic viscosity, μ	0.00029 g/(cm•sec)
Diffusivity, D_{AB}	0.87 cm^2/s
Thermal expansion coefficient, β	0.0017 K^{-1}
Prandtl number, Pr	0.74
Lewis number, Le	0.27
Peclet, Pe	3.02
Concentration number, Cv	1.05
Total system pressure, P_T	248 Torr
Thermal Grashof number, Gr_t	8.5×10^3
Solutal Grashof number,Gr_s	1.05×10^5

occurs from the process of sealing the ampoule or later degassing of the source material. Because of the inevitable presence of this residual gas, solutal convection occurs. If solutal convection is dominant, the imposed temperature profile has little effect on the growth rate. Conductive wall boundary conditions with a nonlinear thermal profile are considered, while the insulated walls are not considered because it is difficult to obtain in practice and most of vapor growth experiments are performed under the imposed nonlinear thermal profiles to avoid nucleation at the ampoule walls. Figure 3 shows the axial temperature profile given by Eq. (11) with maximum ("hump") between T_s and T_c. To prevent nucleation at the walls an experimental technique to impose a nonlinear thermal profile with a maximum between the crystal and the source, usually referred to as a temperature "hump". This temperature hump could eliminate the problem of vapor supersaturation along the transport path and, thus, of parasitic nucleation at the walls. But, these humps may result in sharp temperature gradients near the crystal region, inducing thermal stresses and a decrease in crystal quality. A temperature hump of 20K with T_s = 329, T_c = 309 is selected for this study.

In Fig. 4 the equilibrium vapor transport pressure profile is obtained from Eq. (12) for the hump thermal profile as shown in Fig. 3. The partial pressures of component A (Hg_2Br_2) at the walls are gained from diffusive-convective transport at the horizontal orientation with $1g_0$ and Ar (aspect ratio: transport length-to-width) of 6. It is clear that the hump thermal profile is necessary for the prevention of nucleation at the walls and the elimination of supersaturation along the transport path. Note that with a linear temperature profile, the vapor of component A (Hg_2Br_2) is in a supersaturation throughout the ampoule. Fig. 5 shows that axial distribution of partial pressures of component A for a system with the same conditions as for Fig. 4 with D_{AB} = 0.87 cm^2/s, except for a binary diffusion coefficient of 0.087 cm^2/s. The much small value of the diffusion coefficient can be obtained when inert gases of larger molecular weight or hydrogen pairs at higher total pressure. In this study, instead of using either inert gases with larger molecule weight or the hydrogen pairs, the diffusion coefficient of 0.87 cm^2/s in Fig. 4 is intentionally reduced to 0.087 cm^2/s in the case of Fig. 5 for the study of the effects of diffusion transport on axial distribution of partial pressures of component A (Hg_2Br_2). To avoid the parasitic nucleation of the component A near the crystal region, a larger hump profile near the crystal would be necessary, which is realistic in experiments. As shown in Fig. 5, with lower diffusion coefficients, a convection mode is predominant over a diffusion mode so that the occurrence of supersaturation near the crystal region would arise, reflecting a larger hump profile. Under lower gravity environments, the diffusion is dominated so that a smaller hump thermal profile would be quite appropri-

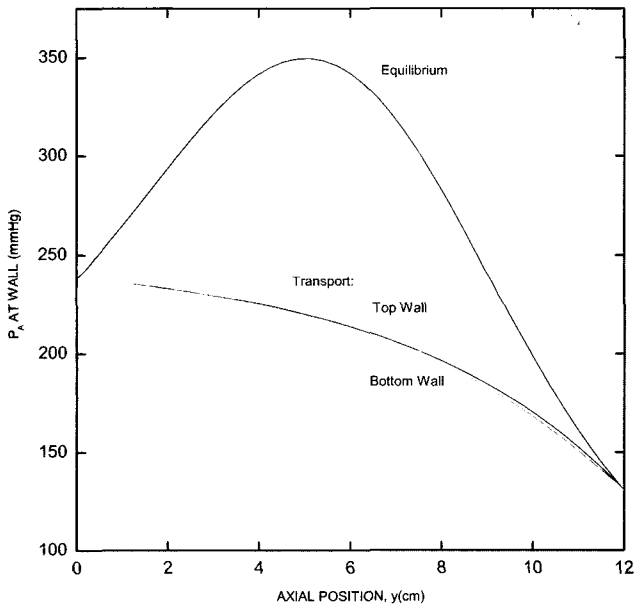

Fig. 4. Axial distribution of partial pressures of component A at the walls resulting from diffusive-convective transport at g_y = $1g_0$, and equilibrium vapor transport pressure, for L/H = 6 and wall temperature profile of Fig. 3.

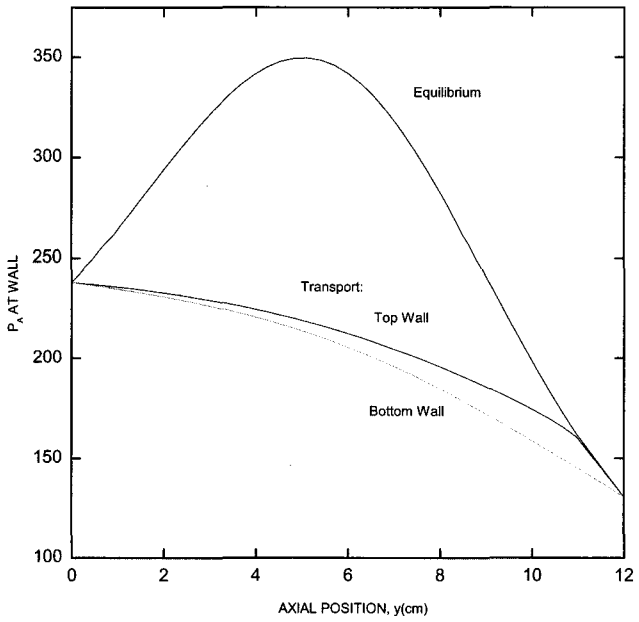

Fig. 5. Axial distribution of partial pressures of component A for system as in Fig. 4 except for D_{AB} = 0.087 cm^2/s.

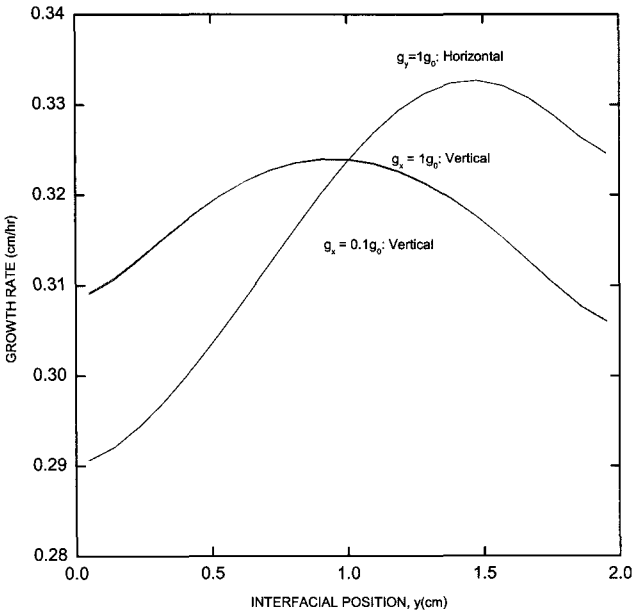

Fig. 6. Interfacial distribution of crystal growth rate of of Hg_2Br_2 for an ampoule aspect ratio 6 and the wall temperature profile of Fig. 3. Horizontal orientation: $g_y = 1g_0$. Vertical orientation: $g_x = 1g_0$, 0.1 g_0.

ate for suppressing the parasitic nucleation near the crystal.

The temperature dependence of the diffusivity on the nonlinear thermal profile is reflected through a binary diffusion coefficient as a function of temperature, which can be calculated from Chapman-Enskog's formula [16]. But, the effect of nonlinear temperature humps would be negligible because of small temperature difference employed.

Figure 6 shows the interfacial distribution of crystal growth rate of Hg_2Br_2 for two different orientations: horizontal ($g_y = 1g_0$), vertical ($g_x = 1g_0$, 0.1 g_0). One sees that convection causes significant nonuniformity near the growing crystals so that it would has a profound influence on the qualities and morphologies of the crystal. The extent of nonuniformity (σ) of the growth rate is defined as

$$\sigma(\%) = \frac{V_{c,max} - V_{c,min}}{V_c} \times 100 \qquad (14)$$

in which $V_{c,max}$ is the local maximum growth rate, $V_{c,min}$ is the local minimum growth rate, and V_c is the average growth rate across the crystal surface. The nonuniformity (σ) here can be considered as the relative magnitude of local Hg_2Br_2 vapor according to the mass flux balances [19]. For the effects of orientation dependence of the growth reactor with respect to gravity on convection, two cases of horizontal and vertical orientations are considered here. The nonuniformity (σ) of the horizontal on earth is 13.2 %, while that of the vertical case with $1g_0$ (on earth) is 5.7 %. As the vertical orientation is switched to the horizontal, the nonuniformity is increased by a factor of 2.3, indicative of the intensity of convection. Also, the growth rate profile is symmetrical across the crystal interfaces, which the diffusion mode is expected to be dominant over the convection mode. Because in particular, for the vertical cases, the growth rate profiles for $1g_0$ and $0.1g_0$ remain nearly unchanged, the diffusion mode is so much dominant that the rate is nearly independent of the gravity levels for the under operating conditions under consideration, as listed in Table 1. In spite of variation of the gravity level for the vertical configurations, the growth rate profile and magnitude are nearly similar, which is intimately related to the effect of the side-walls [20] and relatively low temperature difference imposed under consideration. For the maxima of the growth rates for the two distinct orientations, there are found to be little differences. As not shown here, the parabolic patterns of growth rate distributions indicate one single convection roll occurs toward the growing interface. The convection causes significant nonuniformities in the growth rate across the interface in the crystal region, which is consistent with the results of Markham *et al.* [5]. Therefore, as the intensity of convection increases, the extent of nonuniformity increases as well as the symmetrical extent.

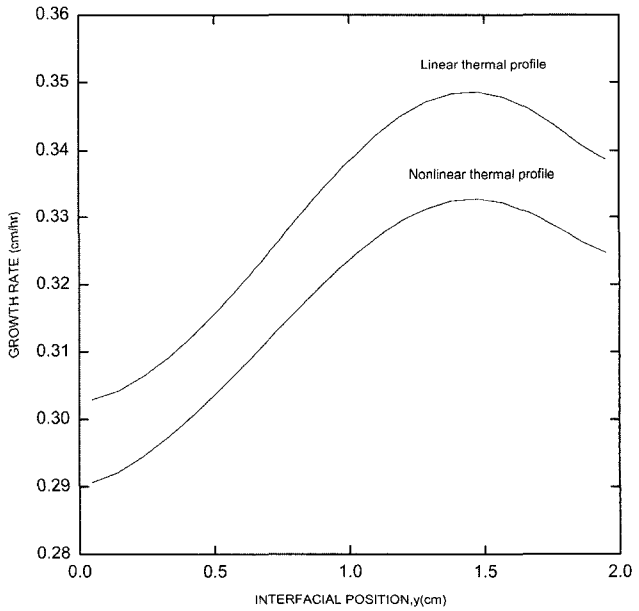

Fig. 7. Interfacial distribution of crystal growth rate of of Hg_2Br_2 for the linear (conducting walls) and nonlinear thermal profiles with an aspect ratio of 6 and the horizontal orientation, $g_y = 1g_0$.

We now investigate the effects of the temperature profile dependence on the growth rate and interfacial distributions across the crystal. Figure 7 illustrates the thermal profile dependence of the growth rate for two cases of linear (conducting walls) and nonlinear thermal profiles. It can be seen that the nonuniformity and growth rate profile are nearly same. For the interfacial positions across the crystal, the rate for linear thermal profile is greater than for the nonlinear by approximately 0.014. The linear thermal profile represents conducting walls, while the nonlinear thermal profile corresponds to the temperature profile with maximum ("hump") between the crystal and source region. Therefore, the linear temperature profile would be applicable to actual experiments instead of the nonlinear profile. As pointed out previously, note that temperature maxima near the crystal are efficient in avoiding the parasitic nucleation near the crystal.

When thermal convection is dominant, i.e., $M_A = M_B$ at $1g_0$ for the horizontal orientation, the results on the growth rate profiles for two different thermal profile are illustrated in Fig. 8. Because the molecular weight of component B is set to be same as that of component A, only thermal convection is considered and the effect of solutal convection arising owing to concentration gradients is neglected. The effect of thermal convection is reflected through density term and binary diffusivity coefficient by setting $M_A = M_B$. Unlike the solutal convection case as shown in Fig. 7, thermal profile has a significant influence on the growth rate and symmetry across the interface. The rate for the linear is much grater than for the nonlinear, and the pattern of growth rate profile for the former is slightly deviated from the latter. The extent of deviation between them is increased with increasing interfacial position to 2 cm. Also, the maximum growth rate of solutal convection for the linear thermal profile is greater than that of thermal convection by about 6.5. Therefore, it is concluded that when the imposed temperature profile has little effect on the growth rate, solutal convection dominates.

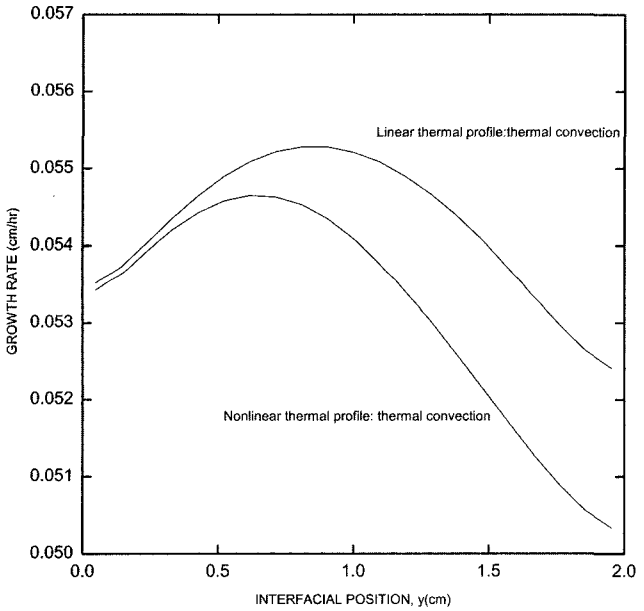

Fig. 8. Interfacial distribution of crystal growth rate of of Hg_2Br_2 for the linear (conducting walls) and nonlinear thermal profiles with an aspect ratio of 6 and the horizontal orientation, $g_y = 1g_0$, thermal convection ($M_A = M_B$).

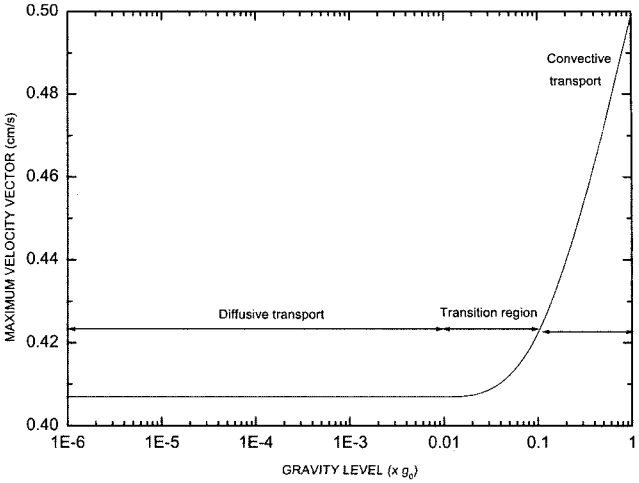

Fig. 9. Growth rates of Hg_2Br_2 as a function of the gravity level (horizontal configuration, $10^{-6}g_0 = g_y = 1g_0$.

Figure 9 shows the effects of gravitational accelerations on the crystal growth rate for the interfacial distributions in a horizontal system of aspect ratio 6 (L = 12 cm, H = 2 cm), with a source temperature T_s = 329, a crystal temperature T_c = 309, an impurity (CO) pressure of 10 Torr. The levels of gravity acceleration ranging between $10^{-6}g_0$ and $1g_0$ are considered for the positive y-direction (horizontal configuration), where g_0 denotes the standard gravitational acceleration constant, 980.665 cm/s^2. For $g_y = 1g_0$, the corresponding dimesionless parameters are thermal Grashof number $Gr_t = 8.5\times10^3$, solutal Grashof number $Gr_s = 1.05\times10^5$, Ar = 6, Pr = 0.74, Le = 0.27 , C_v = 1.05 and Pe = 3.02 with the total pressure of 248 Torr. The maximum magnitude of velocity vector is sharply decreased with a ten reduction of gravitational acceleration near y = 2.0 cm. The maximum velocity vector means the intensity of convection. Two distinct regions are shown. For the microgravity environments less than 0.1 g_0, the magnitude of velocity vector exhibits relatively flat, because the transport is a diffusive mode. For the levels below 0.1 g_0, no

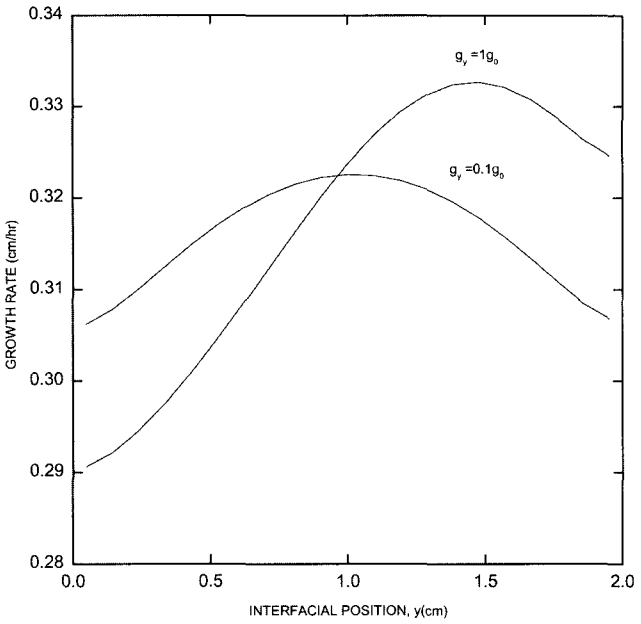

Fig. 10. Interfacial distribution of crystal growth rate of of Hg_2Br_2 for horizontal orientation: g_y = $1g_0$, 0.1 g_0, with Ar (aspect ratio) = 6 and the nonlinear thermal profile of Fig. 3.

recirculating cell is present. Above 10^{-1} g_0, the flow switches to convective mode, and a recirculating cell appears in the vapor phase. Therefore, the study of convection under the microgravity environments provides an important insight of understanding the essence of convection. For gravity levels less than 10^{-1} g_0, the diffusion mode is dominant so that the Stefan wind drives the flow. Therefore, no recircualting cell is predicted for the operating conditions under consideration.

Figure 10 shows the sensitivity of the growth rate to variations of the gravity level for 1 g_0 and 0.1 g_0, at the horizontal configuration. As the convection increases, i.e. the gravity level, the growth rate is increased slightly. For 0.1 g_0, the growth rate profile has a parabolic pattern, which indicates the Stefan wind suppresses the convection mode. Also, the growth rate profile for 0.1 g_0 in Fig. 10 based on the horizontal configuration and the profiles for 1 g_0 and 0.1 g_0 in Fig. 6 with the vertical are nearly similar and their magnitudes are nearly same. It is due to the fact that the diffusion mode is dominant.

4. Conclusions

We concluded that the solutally-driven convection due to the disparity in the molecular weights of the component A (Hg_2Br_2) and B (CO) is stronger than thermally-driven convection for both the nonlinear and the linear thermal profiles, corresponding to $Gr_t = 8.5\times10^3$, $Gr_s = 1.05\times10^5$. For both solutal and thermal convection processes, the growth rates for the linear thermal profile (conducting walls) are greater than for the nonlinear case. But, the effect of the temperature hump has little effect on the growth rate and the nonuniformity. So the results obtained from the linear temperature profile would be applicable as well. Nevertheless, temperature hump near the crystal are found to be most efficient in suppressing parasitic nucleation. With the temperature humps, there are found to be observed in undersaturation for diffusive-convection processes ranging from D_{AB} = 0.087 to 0.87. For the vertical configurations, the diffusion mode is so much dominanted that the growth rate and interfacial distribution is nearly regardless of the gravitational accelerations. Also, the diffusion mode is predominant over the convection for the gravity levels less than 0.1 g_0 for the horizontally-oriented configuration, $Gr_t = 8.5\times10^3$, $Gr_s = 1.05\times10^5$, Ar = 6, Pr = 0.74, Le = 0.27 , C_v = 1.05, Pe = 3.02, P_T = 248 Torr.

Acknowledgement

This work was supported by Korea Sanhak Foundation Grant (2002-2004).

References

[1] N.B. Singh *et al.*, "Growth and characterization of mercurous halide crystals:mercurous bromide system," J. Crystal Growth 137 (1994) 155.
[2] Dworsky and K. Komarek, Monatsh. Chem. 101 (1970) 976.
[3] F. Rosenberger, "Fluid dynamics in crystal growth from vapors," Physico-Chemical Hydro-dynamics 1 (1980) 3.
[4] N.B. Singh *et al.*, "Mercurous Bromide acousto-optic devices", J. Crystal Growth 89 (1986) 173.
[5] B.L. Markham, D.W. Greenwell and F. Rosenberger, "Numerical modeling of diffusive-convective physical vapor transport in cylindrical vertical ampoules," J. Crystal Growth 51 (1981) 426.
[6] Walter M.B. Duval, "Convection in the physical vapor transport process-- I: Thermal," J. Chemical Vapor Deposition 2 (1994) 188.
[7] Walter M.B. Duval, "Transition to chaos in the physical transport process--I," the Proceeding of the ASME--WAM Winter Annual meeting, Fluid mechanics phenomena in microgravity, ASME-WAM, New Orleans, Louisiana, Nov. 28 -- Dec. 3, AMD-174, FED-175, 51 (1993).
[8] A. Nadarajah, F. Rosenberger and J. Alexander, "Effects of buoyancy-driven flow and thermal boundary conditions on physical vapor transport," J. Crystal Growth

118 (1992) 49.
[9] H. Zhou, A. Zebib, S. Trivedi and W.M.B. Duval, "Physical vapor transport of zinc-telluride by dissociative sublimation," J. Crystal Growth 167 (1996) 534.
[10] F. Rosenberger, J. Ouazzani, I. Viohl and N. Buchan, "Physical vapor transport revised," J. Crystal Growth 171 (1997) 270.
[11] N.B. Singh, R. Mazelsky and M.E. Glicksman, "Evaluation of transport conditions during PVT: mercurous chloride system," PhysicoChemical Hydrodynamics No. 1, 11 (1989) 41.
[12] F. Rosenberger and G. Mller, "Interfacial transport in crystal growth, a parameter comparison of convective effects," J. Crystal Growth 65 (1983) 91.
[13] M. Kassemi and Walter M.B. Duval, "Interaction of surface radiation with convection in crystal growth by physical vapor transport," J. Thermophys. Heat Transfer 4 (1989) 454.
[14] N.B. Singh and W.M.B. Duval, "Growth kinetics of physical vapor transport process: crystal growth of the opto-electronic material mercurous chloride", NASA TM 103788 (1991).
[15] C. Mennetrier, W.M.B. Duval and N.B. Singh, "Physical vapor transport process: of mercurous chloride under a nonlinear thermal profile", NASA TM 105920 (1992).
[16] R.B. Bird, W.E. Stewart and E.N. Lightfoot, Transport Phenomena (New York, NY: John Wiley and Sons, 1960).
[17] H. Oppermann, "Chemical aspects of Hg_2X_2-decomposition, barogram-diagram and thermodynamic data", Proceedings of the 2nd Intl symposium on univalent mercury halides, Czecoslovakia (1989).
[18] S.V. Patankar, Numerical Heat Transfer and Fluid flow (New York, NY: McGraw-Hill, 1980).
[19] G.T. Kim, W.M.B. Duval, M.E. Glicksman and N.B. Singh, "Thermal convective effects on physical vapor transport growth of mercurous chloride (Hg_2Cl_2) crystals for axisymmertric 2D cylindrical enclosure," Modelling simu. Mater. Sci. Eng. 3 (1995) 331.
[20] I. Catton, "Effect of wall conducting on the stability of a fluid in a rectangular region heated from below," J. Heat Transfer 94 (1972) 446.